Atomic Force Microscopy Reveals the Alternating Subunit Arrangement of the TRPP2-TRPV4 Heterotetramer

Andrew P. Stewart,[†] Graham D. Smith,[‡] Richard N. Sandford,[‡] and J. Michael Edwardson[†*]
[†]Department of Pharmacology, University of Cambridge, Cambridge, United Kingdom; and [‡]Department of Medical Genetics, Cambridge Institute for Medical Research, Addenbrooke's Hospital, Cambridge, United Kingdom

ABSTRACT There is evidence that polycystin-2 (TRPP2) interacts with two other members of the transient receptor potential (TRP) family, TRPC1 and TRPV4. We have previously shown that TRPP2 forms a heteromeric complex with TRPC1, with a 2:2 stoichiometry and an alternating subunit arrangement. Here, we used coimmunoprecipitation to show that TRPP2 also interacts with TRPV4, but not with TRPA1 or TRPM8; hence, its promiscuity is limited. We then used atomic force microscopy to study the structure of the TRPV4 homomer and the interaction between TRPP2 and TRPV4. The molecular volume of V5-tagged TRPV4 isolated from singly-transfected tsA 201 cells indicated that it assembled as a homotetramer. The distribution of angles between pairs of anti-V5 antibodies bound to TRPV4 particles had a large peak close to 90° and a smaller peak close to 180°, again consistent with the assembly of TRPV4 as a homotetramer. In contrast, the angle distributions for decoration of the TRPP2-TRPV4 heteromer by either anti-Myc or anti-V5 antibodies had major peaks close to 180°. This result indicates that TRPP2-TRPV4 assembles identically to TRPP2-TRPC1, suggesting a common subunit arrangement among heteromeric TRP channels.

INTRODUCTION

Polycystin-2 (TRPP2) is a member of the transient receptor potential (TRP) channel superfamily (1), and has a role in regulating Ca^{2+} efflux from the endoplasmic reticulum (2,3). Importantly, it also interacts with polycystin-1 to form a Ca^{2+}-permeable ion channel complex (4). This complex transduces extracellular mechanical stimuli via the renal primary cilium (5), and regulates multiple intracellular Ca^{2+}-sensitive signaling pathways (4,6). Mutations in TRPP2 and polycystin-1 underlie autosomal dominant polycystic kidney disease (ADPKD), one of the commonest inherited human disorders (reviewed in (7,8)). ADPKD has a population prevalence of over 1:1000 in all ethnic groups, and is a major cause of end-stage renal failure. It is characterized by the progressive development of multiple fluid-filled cysts derived from renal tubular epithelial cells.

In addition to its interaction with polycystin-1, TRPP2 is known to interact with other members of the TRP superfamily, such as TRPC1 (9,10) and TRPV4 (11), and to colocalize with both of these proteins at the primary cilium (10,11). We have recently shown that TRPP2 and TRPC1 form a heterotetramer with a 2:2 stoichiometry and an alternating subunit arrangement (12). The architecture of the TRPP2-TRPC1 heteromer was determined using a method based on atomic force microscopy (AFM) imaging (13–15). The method involves engineering specific epitope tags, including His_6, onto each subunit and expressing the proteins in a suitable cell line (e.g., tsA 201). Crude membrane fractions from the transfected cells are solubilized in detergent, and the proteins are isolated through binding to Ni^{2+}-agarose beads. The proteins are incubated with antibodies to the tags, and the resulting multimer-antibody complexes are imaged by AFM. Multimers with two bound antibodies are identified, and the angles between the antibodies are measured. A frequency distribution of these angles then reveals the architecture of the multimer.

In this study, we used coimmunoprecipitation to determine the extent of TRPP2's interactions with other members of the TRP channel superfamily. We found that TRPP2 interacts with TRPC1 and TRPV4, as previously demonstrated (9–12), but not with TRPA1 and TRPM8; hence, its promiscuity is limited. We then used AFM imaging to study the interaction of TRPP2 with TRPV4. We show that, as with TRPP2 and TRPC1, TRPP2 and TRPV4 form a heterotetramer with a 2:2 stoichiometry and an alternating subunit arrangement.

MATERIALS AND METHODS

Cell culture

tsA 201 cells (a subclone of human embryonic kidney-293 cells stably expressing the SV40 large T-antigen) were grown in Dulbecco's modified Eagle's medium supplemented with 10% (v/v) fetal calf serum, 100 units/mL penicillin, and 100 μg/mL streptomycin, in an atmosphere of 5% CO_2/air.

Channel constructs

DNA encoding human TRPP2 was subcloned into the pcDNA3.1/Myc-His vector (Invitrogen, Paisley, UK), which produces a protein tagged at its C-terminus with Myc and His_6 epitopes. In addition, the sequence encoding the His_6 tag was deleted from this construct to enable the expression of a protein containing only the Myc epitope. DNA for mouse TRPV4, human TRPC1, rat TRPA1, and rat TRPM8, all tagged at their C-termini with V5 and His_6 epitopes, were expressed in the pcDNA3.1/V5-His-TOPO vector (Invitrogen). The TRPV4, TRPA1, and TRPM8 constructs were a kind gift of Dr. Xuming Zhang (Department of Pharmacology, University of Cambridge).

Submitted March 20, 2010, and accepted for publication May 6, 2010.

*Correspondence: jme1000@cam.ac.uk

Editor: Ian Parker.

0006-3495/10/08/0790/8 $2.00

doi: 10.1016/j.bpj.2010.05.012

Transient transfection of tsA 201 cells

Transient transfections of tsA 201 cells with DNA were carried out using the CalPhos mammalian transfection kit (Clontech, Basingstoke, UK), according to the manufacturer's instructions. A total of 250 μg of DNA was used to transfect cells in 5 $\times$ 162 cm^2 culture flasks. When cells were doubly transfected, 125 μg of DNA for each construct was used. After transfection, cells were incubated for 24–48 h at 37°C, to allow protein expression. Protein expression and intracellular localization were checked using immunofluorescence analysis of small-scale cultures. Cells were fixed, permeabilized, and incubated with appropriate primary antibodies (mouse monoclonal anti-Myc and anti-V5, from Invitrogen; mouse monoclonal anti-HA, from Covance, Basel, Switzerland; rabbit polyclonal anti-Myc, from Abcam, Cambridge, UK), followed by either Cy3- or fluorescein isothiocyanate-conjugated goat secondary antibodies (Sigma-Aldrich, Poole, UK). Cells were imaged by confocal laser scanning microscopy.

Coimmunoprecipitation of TRPP2 with other members of the TRP channel superfamily

TRPP2 was coexpressed with TRPC1, TRPV4, TRPA1, or TRPM8 by transient transfection of tsA 201 cells. TRPP2 was immunoprecipitated using a rabbit polyclonal anti-Myc antibody, and its partner protein was immunoprecipitated using a mouse monoclonal anti-V5 antibody. A mouse monoclonal anti-HA antibody was used as a negative control. Immunoprecipitates were analyzed by SDS-polyacrylamide gel electrophoresis followed by immunoblotting, using mouse monoclonal anti-Myc or anti-V5 antibodies.

Solubilization and purification of His_6-tagged proteins

The solubilization/purification procedure was as described previously (13). Briefly, a crude membrane fraction prepared from the cells was solubilized in 1% (w/v) 3-[(3-cholamidopropyl)dimethylammonio]-1-propanesulfonate, and the solubilized material was incubated with Ni^{2+}-agarose beads (Probond, Invitrogen). The beads were washed extensively, and bound proteins were eluted with increasing concentrations of imidazole. Samples were analyzed by SDS-polyacrylamide gel electrophoresis, and proteins were detected by immunoblotting, using mouse monoclonal antibodies against Myc (TRPP2) or V5 (TRPV4), or a rabbit polyclonal antibody against His_6 (TRPP2 and TRPV4; Research Diagnostics, Flanders, NJ).

AFM imaging of TRP proteins and TRP-antibody complexes

Isolated channels were imaged either alone or after overnight incubation at 4°C with a 1:2 molar ratio (~0.2 nM channel protein concentration) of anti-epitope tag monoclonal antibody (Invitrogen). Proteins were diluted to a final concentration of 0.04 nM, and 45 μL of the sample was allowed to adsorb to freshly cleaved, poly-L-lysine-coated mica disks. After a 5-min incubation, the sample was washed with BPC-grade water (Sigma-Aldrich) and dried under nitrogen. Imaging was performed with a Multimode atomic force microscope controlled by a Nanoscope IIIa controller (Veeco Digital Instruments, Santa Barbara, CA). Samples were imaged in air, using tapping mode. The silicon cantilevers used had a drive frequency ~300 kHz and a specified spring constant of 40 N/m (Olympus, Tokyo, Japan). The applied imaging force was kept as low as possible ($A_s/A_0 \sim 0.85$).

The molecular volumes of the protein particles were determined from particle dimensions based on AFM images. After adsorption of the channels onto the mica support, the particles adopt the shape of a spherical cap. As described previously (13), the heights and radii were measured from multiple cross-sections of the same particle, and the molecular volume was calculated using the equation

$$V_m = (\pi h/6)\left(3r^2 + h^2\right), \quad (1)$$

where h is the particle height and r is the radius.

Molecular volume based on molecular mass was calculated using the equation

$$V_c = (M_0/N_0)(V_1 + dV_2), \quad (2)$$

where M_0 is the molecular mass, N_0 is Avogadro's number, V_1 and V_2 are the partial specific volumes of particle (0.74 cm^3/g) and water (1 cm^3/g), respectively, and d is the extent of protein hydration (taken as 0.4 g water/g protein).

RESULTS

The tsA 201 cells were transiently transfected with DNA encoding Myc/His_6-tagged TRPP2 or V5/His_6-tagged TRPC1, TRPV4, TRPA1, or TRPM8. Protein expression and localization was confirmed by immunofluorescence, using appropriate anti-tag antibodies. The staining signals with either anti-Myc or anti-V5 antibodies showed the expression of all five channels (Fig. 1 *A*, *left-hand* and *center panels*). In contrast, use of an anti-HA antibody as a negative control produced only background immunofluorescence signals (Fig. 1 *A*, *right-hand panels*). Bright-field imaging indicated that in all cases the tsA 201 cells were confluent (data not shown); hence, the transfection efficiency was 20–30%.

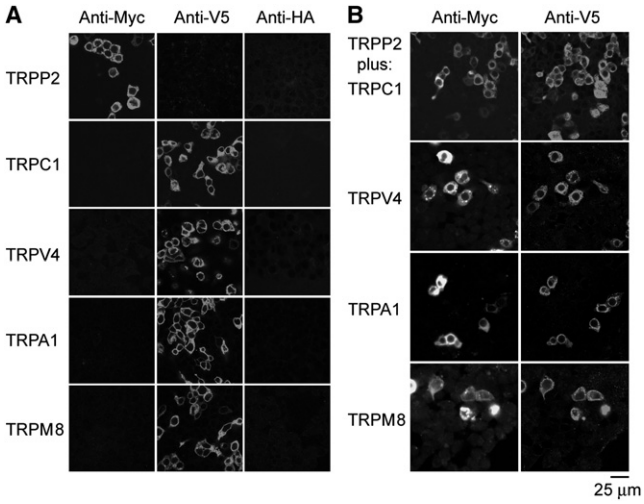

FIGURE 1 Expression of TRP channels in tsA 201 cells. (*A*) Cells were transiently transfected with DNA encoding Myc/His_6-tagged TRPP2 or V5/His_6-tagged TRPV4, TRPC1, TRPA1, or TRPM8. Cells were fixed, permeabilized, and incubated with mouse monoclonal anti-Myc, anti-V5, or anti-HA (control) antibodies, followed by Cy3-conjugated goat anti-mouse secondary antibody. Cells were imaged by confocal laser scanning microscopy. (*B*) Cells were doubly transfected with TRPP2-Myc/His_6 in addition to V5/His_6-tagged TRPV4, TRPC1, TRPA1, or TRPM8. Cells were fixed, permeabilized, and incubated with rabbit polyclonal anti-Myc or mouse monoclonal anti-V5 antibodies, followed by Cy3-conjugated goat anti-rabbit or fluorescein isothiocyanate-conjugated goat anti-mouse secondary antibodies. As shown, the anti-Myc and anti-V5 signals extensively overlapped, indicating that the majority of transfected cells expressed both TRPP2 and its partner protein.

Cells cotransfected with TRPP2-Myc/His_6 in addition to V5/His_6-tagged TRPC1, TRPV4, TRPA1, or TRPM8 gave positive immunofluorescence signals with both anti-Myc and anti-V5 antibodies, indicating the presence of the pairs of proteins (Fig. 1 *B*). As shown, the anti-Myc and anti-V5 signals in doubly-labeled cell populations extensively overlapped, indicating that the majority of transfected cells expressed both TRPP2 and its partner protein. Singly transfected cells were seen occasionally, indicating that cross-talk between the fluorescent signals was minimal. The reticular staining patterns suggest that all five channels were localized predominantly in the endoplasmic reticulum.

Crude membrane fractions prepared from cells expressing TRPP2-Myc/His_6 in addition to V5/His_6-tagged TRPC1, TRPV4, TRPA1, or TRPM8 were solubilized in CHAPS detergent (1% w/v). Fractions were then incubated with anti-Myc, anti-V5 or anti-HA (control) antibodies, followed by immunoprecipitation using Protein G-Sepharose. Precipitated samples were subjected to SDS-polyacrylamide gel electrophoresis and immunoblotting using either anti-Myc or anti-V5 antibodies. As shown in Fig. 2, TRPP2 coprecipitated with either TRPC1 or TRPV4, but not with TRPA1 or TRPM8. Coprecipitation of TRPP2 with TRPC1 and TRPV4 is consistent with previous reports that these pairs of proteins interact (9–12). Lack of coprecipitation with TRPA1 and TRPM8 indicates that its interactions within the TRP channel superfamily are not completely promiscuous.

Membrane fractions from cells expressing TRPV4-V5/His_6, or both TRPP2-Myc/His_6 and TRPV4-V5/His_6, were solubilized in 1% CHAPS and proteins were isolated through the binding of the His_6 tags to Ni^{2+}-agarose beads. Isolated proteins were immunoblotted with anti-Myc, anti-V5, or anti-His_6 antibodies. In a fraction from cells expressing TRPV4, the anti-V5 antibody labeled a band at 100 kDa, consistent with the expected size of the TRPV4 subunit, with its epitope tags (Fig. 3 *A*). In a fraction from cells expressing both TRPP2 and TRPV4, the anti-V5 antibody detected the same 100-kDa band (TRPV4), and the anti-Myc antibody labeled a band at 110 kDa, consistent with the expected size of epitope-tagged TRPP2 (Fig. 3 *B*). The anti-His_6 antibody labeled bands at both 100 kDa and 110 kDa in a fraction from the cotransfected cells (Fig. 3 *B*). Hence, the Ni^{2+}-agarose beads successfully captured the appropriate proteins from the transfected cells. Note that on the anti-His_6 immunoblot, the signal was stronger for TRPP2 than for TRPV4. Assuming that the His_6 tags on the two subunits are equally accessible to the anti-His_6 antibody, this result indicates that the isolated fraction contains more TRPP2 than TRPV4.

Proteins isolated from cells expressing TRPV4 and TRPP2-TRPV4 were imaged by AFM. A representative low-magnification AFM image of a sample isolated from TRPV4-expressing cells is shown in Fig. 3 *C*. The image shows a population of relatively large particles, indicating the presence of a predominant protein species. A similar image was obtained from samples prepared from TRPP2-

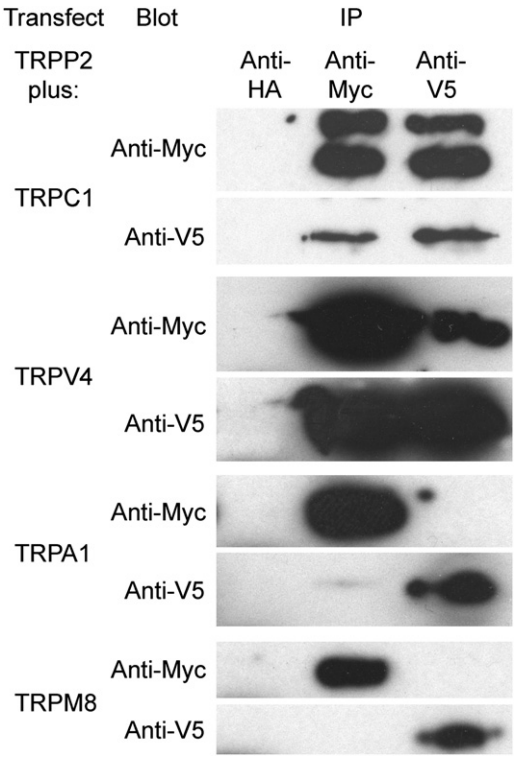

FIGURE 2 Coimmunoprecipitation of TRPP2 with other members of the TRP channel superfamily. TRPP2 was coexpressed with TRPC1, TRPV4, TRPA1, or TRPM8 by transient transfection of tsA 201 cells. Crude membrane fractions prepared from the cells were solubilized in 1% CHAPS. TRPP2 was immunoprecipitated using a rabbit polyclonal anti-Myc antibody, and its partner protein was immunoprecipitated using a mouse monoclonal anti-V5 antibody. A mouse monoclonal anti-HA antibody was used as a negative control. Immunoprecipitates were analyzed by SDS-polyacrylamide gel electrophoresis followed by immunoblotting using mouse monoclonal anti-Myc or anti-V5 antibodies. Immunoreactive bands were visualized using enhanced chemiluminescence.

TRPV4-expressing cells (data not shown). Frequency distributions of molecular volumes were produced for the two sets of particles (Fig. 3, *D* and *E*). The mean molecular volumes were 976 ± 13 (SE) nm^3 ($n = 998$) for TRPV4 (Fig. 3 *D*), and 883 ± 14 nm^3 ($n = 991$) for TRPP2-TRPV4 (Fig. 3 *E*). The molecular volumes predicted for the TRPV4 and TRPP2 subunits on the basis of their molecular mass are 190 nm^3 and 209 nm^3, respectively; hence, a TRPV4 homotetramer would have a predicted molecular volume of 760 nm^3, whereas a TRPP2-TRPV4 heterotetramer would have a predicted molecular volume in the range 779–817 nm^3, depending on the subunit stoichiometry (i.e., 1:3, 2:2, or 3:1). The measured volumes of both TRPV4 and TRPP2-TRPV4, therefore, are consistent with a tetrameric structure, as already demonstrated for TRPC1, TRPP2, and TRPP2-TRPC1 (12). It should be pointed out, though, that measurement of molecular volumes by AFM is complicated by factors such as the convolution introduced by the geometry of the scanning tip. Hence, the measured volume is not by itself a reliable indicator of the stoichiometry of the channel.

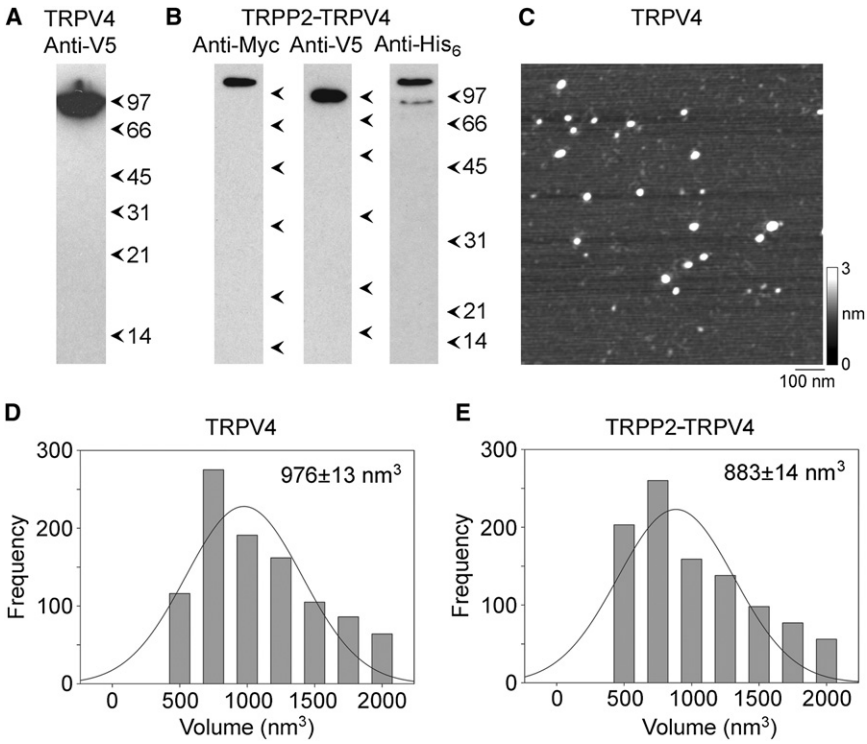

FIGURE 3 Isolation and AFM imaging of TRPV4 homomers and TRPP2-TRPV4 heteromers. (*A* and *B*) Detection of proteins in samples from cells expressing either TRPV4 alone (*A*) or both TRPP2 and TRPV4 (*B*) eluted from Ni^{2+}-agarose columns. Samples were analyzed by SDS-polyacrylamide gel electrophoresis and immunoblotting using anti-tag antibodies, followed by horseradish peroxidase-conjugated goat secondary antibodies. The total yield of isolated proteins was ~500 ng, of which 30 ng was loaded on the gels. (*Arrowheads*) Molecular-mass markers (kDa). (*C*) Low-magnification AFM image of proteins isolated from TRPV4-expressing cells. (*Right*) Shade-height scale. (*D* and *E*) Frequency distributions of molecular volumes of proteins isolated from cells expressing TRPV4 (*D*) and TRPP2-TRPV4 (*E*). (*Curves*) Fitted Gaussian functions. The means of the distributions (± SE) are indicated.

To conclusively establish the stoichiometry of the channels, they were imaged after antibody decoration. TRPV4 was imaged after incubation with anti-V5 antibody (of the immunoglobulin G class), which should decorate the C-terminal V5 epitope tag present on each subunit. A low-magnification AFM image of TRPV4-antibody complexes is shown in Fig. 4 *A*. Several large particles can be seen, some of which have been decorated by either one (*arrowhead*) or two (*arrows*) smaller particles. The small particles had a molecular volume of ~220 nm^3, close to the expected volume of 285 nm^3 for an immunoglobulin G molecule, of molecular mass 150 kDa. Hence, these particles represent anti-V5 antibodies bound to the V5 epitopes on the TRPV4 channel. A gallery of undecorated, singly-, and doubly-decorated large particles is shown in Fig. 4 *B*, along with an example of a triply-decorated large particle. Of 1156 large particles imaged, 713 (61.7%) were undecorated, 369 (31.9%) were singly-decorated, 72 (6.2%) were doubly-decorated, and 2 (0.2%) were triply-decorated. No quadruply decorated channels were seen. This antibody decoration profile is similar to that predicted by the binomial distribution for an 11% occupancy of all potential binding sites (calculated assuming that the channel is a tetramer).

We identified TRPV4 channels that had been decorated by two or three antibodies and then measured the angles between the bound antibodies. This was done in each case by joining the highest point on the central particle (the TRPV4 channel) to the highest points on the peripheral particles (the antibodies) by lines and then determining the angle between the two lines. The frequency distribution of angles obtained is shown in Fig. 4 *C*. The angle distribution has two peaks: a large peak at 98 ± 2° and a smaller peak at 176 ± 14°. The ratio of the numbers of particles within the two peaks is 1.9:1. For a homotetramer, the expected result is a distribution with peaks at 90° and 180° in the ratio 2:1, close to the observed ratio. In contrast, a trimer would give a single angle peak at 120° (13), whereas a pentamer would give equally sized peaks at 72° and 144° (15). Hence, the antibody decoration profile confirms that TRPV4 assembles as a homotetramer.

When proteins isolated from cells expressing both TRPP2-Myc/His_6 and TRPV4-V5/His_6 were incubated with anti-Myc or anti-V5 antibodies and then imaged by AFM, antibody-decorated large particles were again seen. A gallery of zoomed images of undecorated particles, and particles that had been singly- or doubly-decorated by either anti-Myc or anti-V5 antibodies, is shown in Fig. 5 *A*. Of 1752 large particles imaged, 47 (2.7%) were doubly decorated by anti-Myc antibodies. Similarly, of 1821 large particles imaged, 56 (3.1%) were doubly-decorated by anti-V5 antibodies. No triply or quadruply decorated particles were seen for either anti-Myc or anti-V5 antibodies.

The angles between the pairs of bound antibodies were measured and used to construct frequency distributions. As for the TRPV4 homomer, both distributions had two peaks (Fig. 5 *B*). However, in marked contrast to the results for the homomer, the smaller peak was at 83 ± 2° for anti-Myc and 87 ± 3° for anti-V5, whereas the larger peak was at 163 ± 2° for anti-Myc and 175 ± 11° for anti-V5. The ratios of the numbers of particles within the two peaks were 1:1.8 for anti-Myc and 1:2.3 for anti-V5. These distributions show

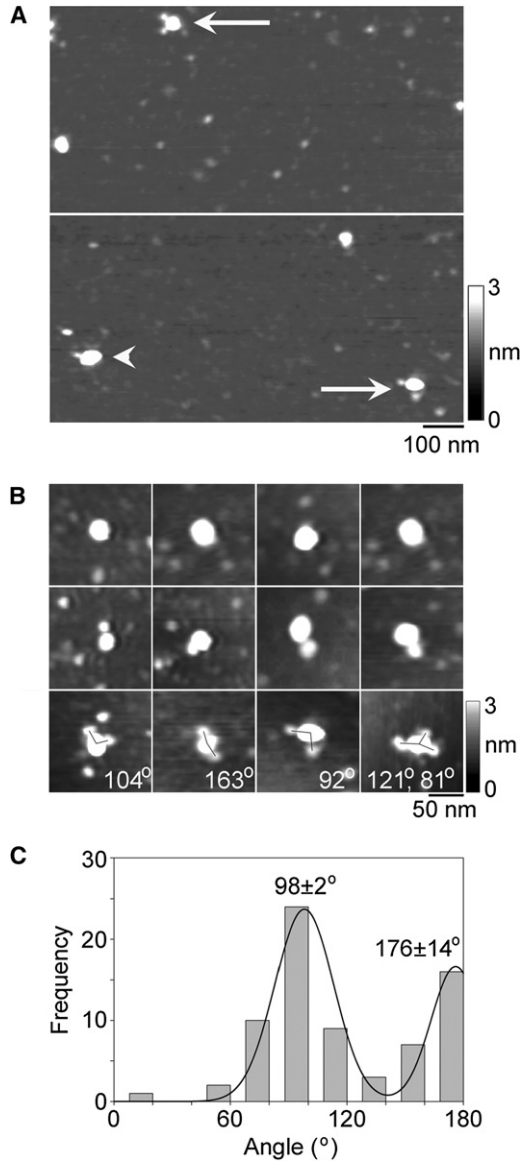

FIGURE 4 Decoration of TRPV4 channels with anti-Myc antibodies. (*A*) Low-magnification AFM images of a sample of isolated TRPV4 that had been incubated with anti-Myc antibodies. (*Arrowhead*) Singly-decorated TRPV4 particle. (*Arrows*) Doubly-decorated particles. (*Right*) Shade-height scale. (*B*) Gallery of zoomed images of TRPV4 particles that are undecorated (*top*), or decorated by one (*middle*) or two (*bottom*) peripheral particles (antibodies). One triply decorated particle is also shown. Angles between pairs of antibodies are indicated. (*Right*) Shade-height scale. (*C*) Frequency distribution of angles between pairs of bound antibodies. The curve indicates the fitted Gaussian functions. The peaks of the distribution are indicated.

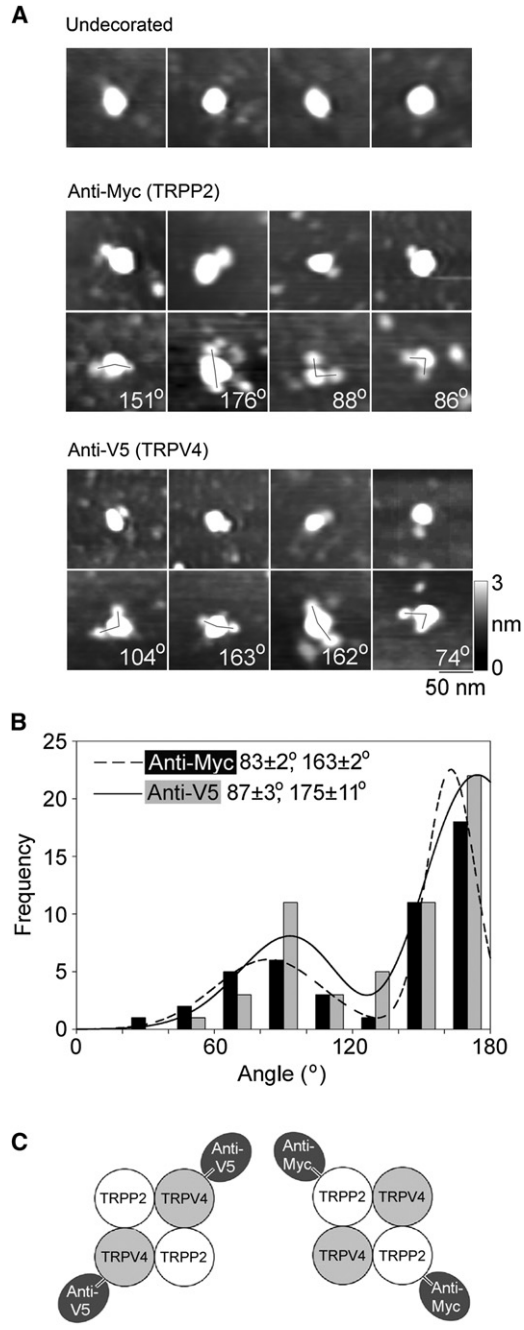

FIGURE 5 Decoration of TRPP2-TRPV4 channels with anti-Myc and anti-V5 antibodies. (*A*) Gallery of zoomed images of particles that are undecorated (*top*), decorated by one or two anti-Myc antibodies (*middle*), or decorated by one or two anti-V5 antibodies (*bottom*). Angles between pairs of antibodies are indicated. (*Right*) Shade-height scale. (*B*) Frequency distributions of angles between pairs of bound anti-Myc and anti-V5 antibodies. The curves indicate the fitted Gaussian functions. The peaks of the distributions are indicated. (*C*) (*Diagram*) Predominant subunit arrangement within the TRPP2-TRPV4 heteromer, as revealed by the antibody decoration patterns.

a strong preference for decoration of the TRPP2-TRPV4 heteromer at ~180°, indicating a predominantly alternating subunit arrangement, as illustrated in Fig. 4 *C*.

The TRPP2-TRPV4 heteromer showed small antibody decoration peaks at 90°, for both Myc and V5 epitope tags. These peaks could result from the isolation of minor populations of TRPP2 and TRPV4 homomers from the TRPP2-TRPV4-transfected cells. This is especially likely for TRPP2, because the anti-His_6 antibody immunoblot (Fig. 3 *B*) suggested that the protein fraction prepared from cotransfected cells contained more TRPP2 than TRPV4.

Alternatively, they could indicate that the architecture of the heteromer is not invariant, and that some of the heteromers assemble with a TRPP2-TRPP2-TRPV4-TRPV4 arrangement. To distinguish between these two possibilities, we expressed a combination of TRPP2-Myc (lacking a His_6 tag) and TRPV4-V5/His_6 in the tsA 201 cells. The normal isolation procedure was then used to produce protein complexes containing TRPV4-V5/His_6. Isolated proteins were then incubated with anti-Myc antibodies, which would decorate only heteromeric complexes containing TRPP2-Myc. Of 2047 large particles imaged, 48 (2.3%) were doubly decorated by anti-Myc antibodies. In a control experiment, we incubated the isolated channels with anti-HA antibody. Now only 0.4% of the large particles were doubly decorated; hence, the vast majority of the double decoration events seen with anti-Myc were specific. A gallery of protein complexes doubly decorated with anti-Myc is shown in Fig. 6 *A*. All the angles were now ~180°. Gaussian fitting showed that the frequency distribution of angles between pairs of bound antibodies (Fig. 6 *B*) had only a single peak, at 161 ± 5° ($n = 48$); the peak at ~90° seen previously was not present. This result indicates that the heteromer assembles with the exclusive subunit arrangement TRPP2-TRPV4-TRPP2-TRPV4, and that the 90° peak was a result of the presence of a minority of homotetramers in the isolates from cells expressing both TRPP2-Myc/His_6 and TRPV4-V5/His_6.

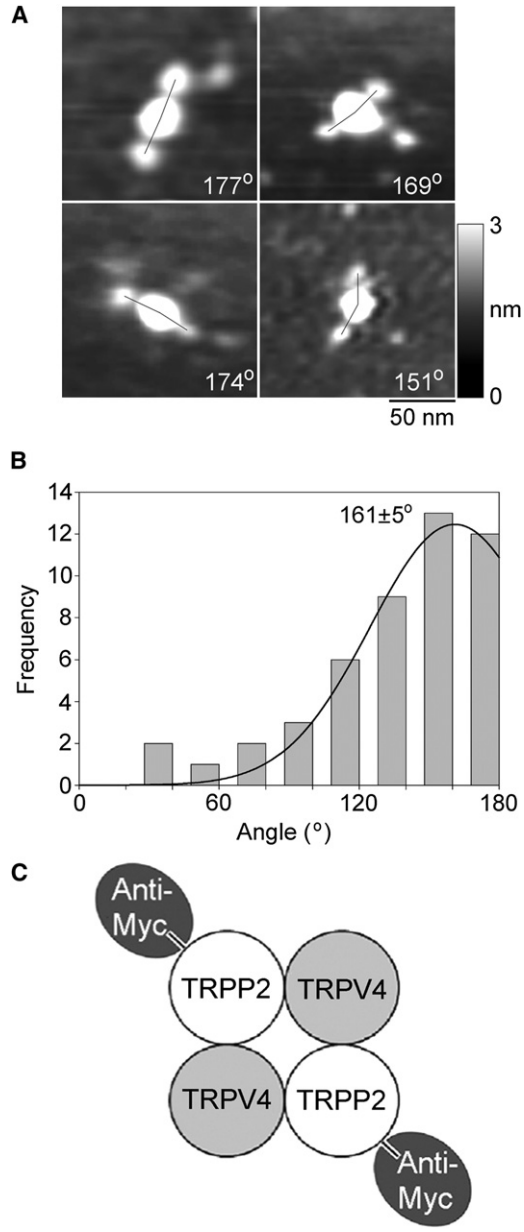

FIGURE 6 Decoration of TRPP2-TRPV4 channels isolated from cells expressing TRPP2-Myc and TRPV4-V5/His_6 with anti-Myc antibodies. (*A*) Gallery of zoomed images of particles decorated by two anti-Myc antibodies. Angles between pairs of antibodies are indicated. (*Right*) Shade-height scale. (*B*) Frequency distributions of angles between pairs of bound anti-Myc antibodies. (*Curve*) Fitted Gaussian function. The peak of the distribution is indicated. (*C*) (*Diagram*) Subunit arrangement within the TRPP2-TRPV4 heteromer, as revealed by the antibody decoration pattern.

DISCUSSION

TRPP2 has been shown previously to interact with both TRPC1 (9,10) and TRPV4 (11). These interactions have been detected by coimmunoprecipitation and fluorescence resonance energy transfer, and through the demonstration that coexpression of two different subunits produces channels with properties distinct from those formed after expression of either subunit alone. TRPP2 and TRPV4 are coexpressed at the primary cilium of renal epithelial cells, and the two proteins form a mechano- and thermosensor (11). Depletion of TRPV4 abolishes flow-induced Ca^{2+} transients, suggesting that the two proteins are key components of the ciliary mechanosensor. Significantly, however, TRPV4-deficient zebrafish and TRPV4 knockout mice do not develop cysts, suggesting that the TRPP2-TRPV4 complex is not involved in the etiology of ADPKD. This is not to say that TRPV4 is completely uninvolved in cystic disease, as cholangiocyte hyperproliferation can be reduced in a mouse model of autosomal recessive polycystic kidney disease using TRPV4 agonists (16).

In this study, we have confirmed the observations that TRPP2 coimmunoprecipitates with TRPC1 and TRPV4. In addition, we show that the promiscuity of TRPP2's interactions is limited; for instance, it does not interact with representatives of the TRPA and TRPM channel families. This selectivity has also been reported for members of the TRPC family, where TRPC1 interacts with TRPC4 and 5, and TRPC3, 6 and 7 are also able to form heteromers, whereas TRPC2 only forms homomers (17). The structural basis of these selective interactions is so far obscure. The interaction between TRPP2 and TRPC1 was mapped to two regions of TRPP2: the cytosolic C-terminus, and a larger region including transmembrane regions 2–6 and the connecting loops (9). However, why TRPP2 interacts with TRPC1 and TRPV4 but not with TRPA1 or TRPM8 is not known.

Several techniques, including cryo-electron microscopy, fluorescence resonance energy transfer and chemical cross-linking have been used to show that various TRP channels, including TRPC1 (14), TRPC3 (18), TRPV1 (19,20), TRPV5 and TRPV6 (21), and TRPM2 (22) assemble as tetramers. Here we used antibody decoration of epitopes on TRPV4 subunits to demonstrate that TRPV4, too, forms homotetramers. This result is in agreement with the recent findings of Shigematsu et al. (23) using cryo-EM. As far as we are aware, the only exceptions to this pattern of tetrameric assembly of TRP channels are the recent reports of a trimeric structure for TRPP2, based in part on the behavior of isolated C-terminal fragments (24,25). These results conflict with our demonstration, again based on antibody decoration, that TRPP2, like the other channels listed above, is tetrameric (12).

Although we used equal amounts of DNA for the two constructs when expressing the TRPP2/TRPV4 heteromer, the isolated fraction apparently contained more TRPP2 than TRPV4. Nevertheless, the heteromer assembled with a 2:2 stoichiometry and alternating subunit arrangement, suggesting that this arrangement might be the preferred assembly state for the heteromeric channel. This suggestion is supported by our recent demonstration that TRPP2 also assembles with TRPC1 to form a heteromeric channel with alternating subunits (12). As yet, however, we cannot exclude the possibility that the subunit stoichiometry of the heteromer is not fixed, but rather can be manipulated by changing the relative expression levels of the two subunits, as we have previously found for the P2X2/P2X6 receptor heteromer (26).

We are now in a position to test the generality of our proposed model for the assembly of heteromeric TRP channels by applying our AFM-based method to other pairs of interacting subunits. It should also be possible to use mutational analysis to determine the regions responsible for the apparent preferential interactions between different subunits, such as TRPP2 and TRPV4. Clinical mutations affecting homomeric and heteromeric assembly of TRPP2 have been identified. These include a truncation of the C-terminal tail of TRPP2 that triggers its interaction with TRPC3 and TRPC7 (27). Using our AFM-based approach, we ought to be able to begin to understand the molecular mechanisms underlying the assembly of TRP channel heteromers. Of most relevance to the etiology of ADPKD, of course, is the interaction of TRPP2 with polycystin-1. We hope that AFM imaging might also allow us to determine the architecture of the complex formed between these two proteins.

We thank Dr. Xuming Zhang for providing the TRPV4, TRPA1, and TRPM8 expression vectors.

A.P.S. is a member of the University of Cambridge MB/PhD Program, and is supported by the Jean Shanks Foundation and the James Baird Fund. G.D.S. is supported by the National Institutes of Health Research Cambridge Biomedical Research Centre. J.M.E. and R.N.S. are supported by Kidney Research UK.

REFERENCES

1. Mochizuki, T., G. Wu, T. Hayashi, …, S. Somlo. 1996. PKD2, a gene for polycystic kidney disease that encodes an integral membrane protein. *Science*. 272:1339–1342.
2. Geng, L., W. Boehmerle, …, S. Somlo. 2008. Syntaxin 5 regulates the endoplasmic reticulum channel-release properties of polycystin-2. *Proc. Natl. Acad. Sci. USA*. 105:15920–15925.
3. Wegierski, T., D. Steffl, …, M. Köttgen. 2009. TRPP2 channels regulate apoptosis through the Ca^{2+} concentration in the endoplasmic reticulum. *EMBO J*. 28:490–499.
4. Hanaoka, K., F. Qian, …, G. G. Germino. 2000. Co-assembly of polycystin-1 and -2 produces unique cation-permeable currents. *Nature*. 408:990–994.
5. Nauli, S. M., F. J. Alenghat, …, J. Zhou. 2003. Polycystins 1 and 2 mediate mechanosensation in the primary cilium of kidney cells. *Nat. Genet*. 33:129–137.
6. Delmas, P., S. M. Nauli, …, J. Zhou. 2004. Gating of the polycystin ion channel signaling complex in neurons and kidney cells. *FASEB J*. 18:740–742.
7. Yoder, B. K., S. Mulroy, …, R. Sandford. 2006. Molecular pathogenesis of autosomal dominant polycystic kidney disease. *Expert Rev. Mol. Med*. 8:1–22.
8. Harris, P. C., and V. E. Torres. 2009. Polycystic kidney disease. *Annu. Rev. Med*. 60, 27.1–27.17.
9. Tsiokas, L., T. Arnould, …, V. P. Sukhatme. 1999. Specific association of the gene product of PKD2 with the TRPC1 channel. *Proc. Natl. Acad. Sci. USA*. 96:3934–3939.
10. Bai, C.-X., A. Giamarchi, …, P. Delmas. 2008. Formation of a new receptor-operated channel by heteromeric assembly of TRPP2 and TRPC1 subunits. *EMBO Rep*. 9:472–479.
11. Köttgen, M., B. Buchholz, …, G. Walz. 2008. TRPP2 and TRPV4 form a polymodal sensory channel complex. *J. Cell Biol*. 182:437–447.
12. Kobori, T., G. D. Smith, …, J. M. Edwardson. 2009. The transient receptor potential (TRP) channels TRPP2 and TRPC1 form a heterotetramer with a 2:2 stoichiometry and an alternating subunit arrangement. *J. Biol. Chem*. 284:35507–35513.
13. Barrera, N. P., S. J. Ormond, …, J. M. Edwardson. 2005. AFM imaging demonstrates that $P2X_2$ receptors are trimers, but that $P2X_6$ receptor subunits do not oligomerize. *J. Biol. Chem*. 280:10759–10765.
14. Barrera, N. P., Y. Shaifta, …, J. M. Edwardson. 2007. AFM imaging reveals the tetrameric structure of the TRPC1 channel. *Biochem. Biophys. Res. Commun*. 358:1086–1090.
15. Barrera, N. P., P. Herbert, …, J. M. Edwardson. 2005. Atomic force microscopy reveals the stoichiometry and subunit arrangement of 5-HT_3 receptors. *Proc. Natl. Acad. Sci. USA*. 102:12595–12600.
16. Gradilone, S. A., T. V. Masyuk, …, N. F. Larusso. 2010. Activation of Trpv4 reduces the hyperproliferative phenotype of cystic cholangiocytes from an animal model of ARPKD. *Gastroenterology*. 10.1053/j.gastro.2010.04.010.
17. Hofmann, T., M. Schaefer, …, T. Gudermann. 2002. Subunit composition of mammalian transient receptor potential channels in living cells. *Proc. Natl. Acad. Sci. USA*. 99:7461–7466.
18. Mio, K., T. Ogura, …, C. Sato. 2007. The TRPC3 channel has a large internal chamber surrounded by signal sensing antennas. *J. Mol. Biol*. 367:373–383.
19. Kedei, N., T. Szabo, …, P. M. Blumberg. 2001. Analysis of the native quaternary structure of vanilloid receptor 1. *J. Biol. Chem*. 276:28613–28619.
20. Moiseenkova-Bell, V. Y., L. A. Stanciu, …, T. G. Wensel. 2008. Structure of TRPV1 channel revealed by electron cryomicroscopy. *Proc. Natl. Acad. Sci. USA*. 105:7451–7455.
21. Hoenderop, J. G. J., T. Voets, …, R. J. Bindels. 2003. Homo- and heterotetrameric structure of the epithelial Ca^{2+} channels TRPV5 and TRPV6. *EMBO J*. 22:776–785.

22. Maruyama, Y., T. Ogura, …, C. Sato. 2007. Three-dimensional reconstruction using transmission electron microscopy reveals a swollen, bell-shaped structure of transient receptor potential melastatin type 2 cation channel. *J. Biol. Chem.* 282:36961–36970.

23. Shigematsu, H., T. Sokabe, …, K. Nagayama. 2009. A 3.5-nm structure of rat TRPV4 cation channel revealed by Zernike phase-contrast cryo-EM. *J. Biol. Chem.* 285:11210–11218.

24. Yu, Y., M. H. Ulbrich, …, J. Yang. 2009. Structural and molecular basis of the assembly of the TRPP2/PKD1 complex. *Proc. Natl. Acad. Sci. USA.* 106:11558–11563.

25. Molland, K. L., A. Narayanan, …, D. A. Yernool. 2010. Identification of the structural motif responsible for trimeric assembly of the carboxyl-terminal regulatory domains of polycystin channels PKD2L1 and PKD2. *Biochem. J.* 429:171–183.

26. Barrera, N. P., R. M. Henderson, …, J. M. Edwardson. 2007. The stoichiometry of $P2X_{2/6}$ receptor heteromers depends on relative subunit expression levels. *Biophys. J.* 93:505–512.

27. Miyagi, K., S. Kiyonaka, …, Y. Mori. 2009. A pathogenic C terminus-truncated polycystin-2 mutant enhances receptor-activated Ca^{2+} entry via association with TRPC3 and TRPC7. *J. Biol. Chem.* 284:34400–34412.